Biophysical Journal
Article

Biophysical Society

Crowding affects structural dynamics and contributes to membrane association of the NS3/4A complex

Natalia Ostrowska,[1,2] Michael Feig,[3] and Joanna Trylska[1,*]
[1]Centre of New Technologies, University of Warsaw, Warsaw, Poland and [2]College of Inter-Faculty Individual Studies in Mathematics and Natural Sciences, University of Warsaw, Warsaw, Poland; and [3]Department of Biochemistry and Molecular Biology, Michigan State University, East Lansing, Michigan

ABSTRACT Using molecular dynamics simulations, we describe how crowded environments affect the internal dynamics and diffusion of the hepatitis C virus proteases NS3/4A. This protease plays a key role in viral replication and is successfully used as a target for antiviral treatment. The NS3 enzyme requires a peptide cofactor, called NS4A, with its central part interacting with the NS3 β-sheet, and flexible, protruding terminal tails that are unstructured in water solution. The simulations describe the enzyme and water molecules at atomistic resolution, whereas crowders are modeled via either all-atom or coarse-grained models to emphasize different aspects of crowding. Crowders reflect the polyethylene glycol (PEG) molecules used in the experiments to mimic the crowded surrounding. A bead-shell model of folded coarse-grained PEG molecules considers mainly the excluded volume effect, whereas all-atom PEG models afford more protein-like crowder interactions. Circular dichroism spectroscopy experiments of the NS4A N-terminal tail show that a helical structure is formed in the presence of PEG crowders. The simulations suggest that crowding may assist in the formation of an NS4A helical fragment, positioned exactly where a transmembrane helix would fold upon the NS4A contact with the membrane. In addition, partially interactive PEGs help the NS4A N-tail to detach from the protease surface, thus enabling the process of helix insertion and potentially helping the virus establish a replication machinery needed to produce new viruses. Results point to an active role of crowding in assisting structural changes in disordered protein fragments that are necessary for their biological function.

SIGNIFICANCE Our understanding of biochemical processes largely relies on experiments conducted in dilute solutions, whereas living cells are densely crowded with many macromolecules. We investigate how this dramatic change of environment affects the dynamics of a protein crucial in the replication of the hepatitis C virus. This protein, called NS3/4A, has disordered tails that have to anchor and fold close to the human endoplasmic reticulum membrane. Using simulations and experiments, we found that crowding aids folding of the NS3/4A unstructured tails, suggesting that it contributes to NS3/4A membrane anchoring. The results bring us closer to answering the question of how cellular crowding modulates the behavior observed during in vitro biochemical experiments and simulations.

INTRODUCTION

The natural environment in which proteins perform their function is highly crowded with macromolecules such as nucleic acids, proteins, lipids, and small molecules such as metabolites and cosolutes. This heterogeneous molecular crowd typically occupies 20–30% of the cytoplasmic volume but can reach up to 80% in the extracellular matrix. The practical consequence of crowding is that biochemical reactions inside living organisms proceed differently from those observed in a test tube, where experiments typically involve dilute buffer conditions. Crowder molecules affect various properties of solutes; they can reduce their diffusion and may influence folding, internal dynamics and stability, association and formation of molecular complexes, ligand and substrate binding, or the catalytic activity of enzymes (1,2).

Considering the physics of crowding, there are two major components to its effect on proteins: the excluded volume effect, resulting solely from the reduction of the available space, and weak, nonspecific interactions of proteins with the crowder molecules. Because the contribution of each component is case dependent (2), a universal correction to experiments conducted in dilute solutions is difficult to develop.

Submitted February 13, 2021, and accepted for publication July 7, 2021.

*Correspondence: joanna@cent.uw.edu.pl

Editor: Alemayehu Gorfe.

https://doi.org/10.1016/j.bpj.2021.07.008

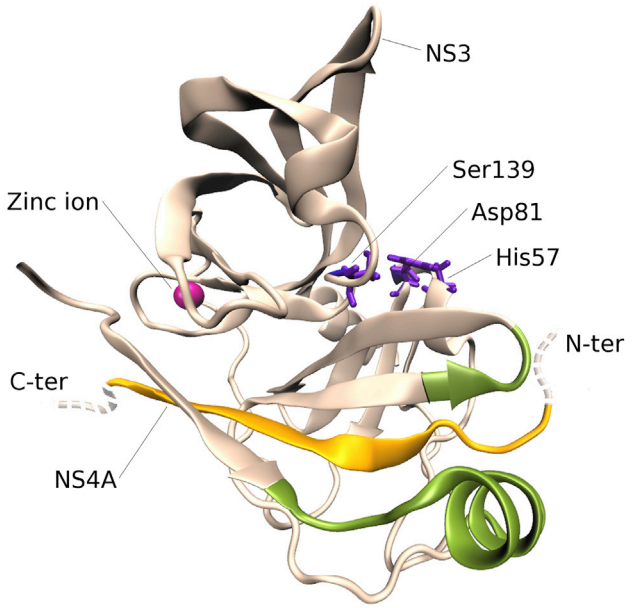

FIGURE 1 Ribbon model of the NS3/4A protease structure (Protein Data Bank: 4JMY). The active site residues are shown in violet, the central crystallographically resolved part of the NS4A cofactor is in yellow, and the NS3 membrane contact sites are in green. C-ter, C-terminus; N-ter, N-terminus. To see this figure in color, go online.

In molecular dynamics (MD) simulations, crowders can be included explicitly, and their representation can focus on specific features. Spherical, noninteracting particles capture the volume-exclusion effect. Such a simplified model leads to stabilized protein-protein interactions (3,4) and promotes compact conformations (5). In a more realistic model, the shape of the crowder particles may be modified or diversified, for example, by mixing spheres with spherocylindrical structures. Such models better represent the entropic part of the crowding effect. However, the mostly attractive nonspecific protein-crowder interactions encountered in biological environments would still be neglected. A more detailed model involves atomistic representations of crowders, although the high computational costs of such simulations limit crowder and overall system sizes (6,7). In laboratory experiments, crowded conditions are typically realized with mostly noninteracting, soluble polymers, such as dextran, Ficoll, or polyethylene glycol (PEG). Solutions with such polymers can be analyzed with a wider range of biophysical methods than a solution of protein-type crowders or cell extracts. However, the polymer choice also determines which crowding effects are emphasized. Synthetic crowders that lack interactions with proteins mostly emphasize the volume-exclusion effect, whereas other polymers such as PEG, for example, that interact weakly with proteins may reflect more closely the behavior of weakly interacting protein crowders (8,9).

Here, we focus on the effects of crowding on the NS3/4A heterodimer protease encoded by the hepatitis C virus (HCV) (Fig. 1). The complex consists of a globular NS3 protease domain and NS4A, a 54 amino acid protein cofactor. The protease cleaves the junctions in the polyprotein produced from viral RNA (10), releasing the nonstructural proteins vital to viral RNA replication and new virion assembly. Because of its key role in the production of new viruses, multiple inhibitors blocking the NS3 activity are currently used in HCV treatment (11,12). NS4A takes part in anchoring the replication machinery to the endoplasmic reticulum (ER) membrane. Because the viral RNA exposed to the cytosol may be vulnerable to degradation by various nucleases, HCV RNA is replicated primarily in the perinuclear ER membrane regions (13) where nonstructural HCV proteins are colocalized. There, safeguarded by a self-made membranous web, new viruses are produced. Consequently, NS4A is another potential target for developing antiviral therapies. The focus on the effect of crowding on NS3 and NS4A aims at providing a more realistic view of their dynamics under biological conditions.

NS4A is an intrinsically disordered peptide (IDP) in solution that is subject to significant conformational fluctuations. The folding or unfolding of IDPs is often dictated by the environment and especially prone to be affected by crowding. A restriction of the available volume often results in compaction of disordered fragments (14), whereas nonspecific interactions with the surrounding molecules can lead to opposite effects (15). Protein crowders may destabilize the native fold of some proteins (6,7), thereby widening the accessible conformational space (16,17). Which specific effect dominates for a given peptide and how biological function may be affected depend on the case.

Many IDPs adopt a stable fold upon contacting a specific binding partner. NS4A is an example of such behavior. The central segment (residues 21–32) of NS4A noncovalently binds to NS3, forming a part of its β-barrel (Fig. 1), although the N- and C-termini (residues 1–22 and 33–54, respectively; Fig. 1) remain unstructured. Moreover, crystallographic structures (18) show that upon binding NS4A, 30 N-terminal amino acids of NS3 rearrange from a random coil into a β-loop and short α-helix. The evolutionary conserved N-terminal segment of NS4A (residues 2–20) are believed to form a transmembrane (TM) α-helix (10) that folds upon interaction with the membrane (19). The TM helix of NS4A, together with the NS3 β-loop and helix, form a three-point contact site that enables binding of the NS3/4A complex to the ER membrane. This event likely establishes HCV foci in the infected cell.

Some of the structural transitions within the viral proteins, including NS4A, are modulated by the molecular environment. In this work, we ask specifically whether crowding can contribute to HCV function by promoting folding of the unstructured tails of NS4A to aid with membrane anchoring. Using circular dichroism (CD) spectroscopy, we investigated the structural changes of the N-terminal fragment of NS4A. The conformational dynamics of the NS3/4A complex is analyzed based on MD simulations under

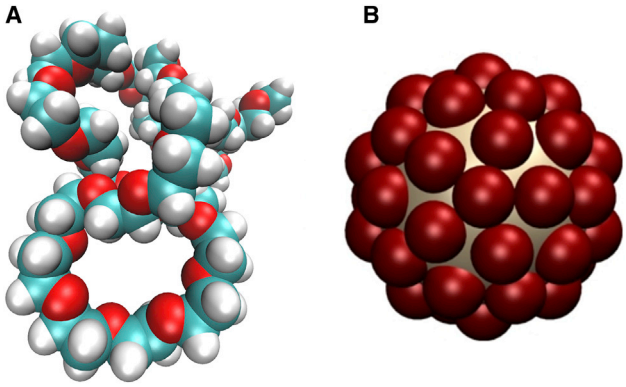

FIGURE 2 Crowder models used in MD simulations: (*A*) an all-atom PEG molecule and (*B*) a CG bead-shell model. During MD simulations, the CG crowder slightly changes shape from a perfect sphere to a dodecahedron (Fig. S1). To see this figure in color, go online.

crowded and noncrowded conditions. By considering different crowder models, we further separated the effects of volume exclusion and crowder-protein interactions. More specifically, we used PEG crowders in atomistic or coarse-grained detail to connect with our previous experiments on NS3/4A under crowded conditions (9).

MATERIALS AND METHODS

Preparation of structures for simulations

The crystal structure of NS3/4A with PDB: 4JMY (20) from the Protein Data Bank was used as a starting point because of its sufficiently high resolution (1.95 Å) and the presence of the zinc ion, which is critical for NS3 structural stability (21). 10 amino acids were mutated to match the sequence of the genotype 1b of HCV because the protease of this genotype was used in our experimental studies (9). The D30E, L36V, G66A, A87K, M94L, S147F, V150A, I170V, A181S, and S182P mutations were introduced with Chimera (22) using the Dunbrack rotamer library (23). In initial MD simulations, these mutations did not affect the structural properties of NS3. Standard protonation states for amino acids at pH 7 were assumed. Histidines were set to their neutral τ tautomer form with the H-bond acceptor at the Nϵ position. For cysteines 97, 99, and 145, which coordinate the zinc ion (10), we used a cysteine-zinc specific patch. The total net charge of the NS3/4A complex plus the zinc ion was +2e. Only the central part of NS4A (residues 21–32) was resolved in the crystal structure of NS3/4A (20). Missing terminal fragments of NS4A were built with MODELLER (24), ver. 9.19., using template-free modeling. From five models of full-length NS4A, the best model was selected based on the scores calculated with Dope (25). A peptide composed of 22 N-terminal amino acids of NS4A (N_{ter}-STWVLVGGVLAALAAYCLTTGS-C_{ter}) was simulated starting from helical (built with Chimera (22)) and extended conformations (from the NS3/4A simulations).

Simulation systems

NS3/4A was simulated in noncrowded and crowded conditions. Crowded conditions involved PEG molecules either in all-atom representation or as CG crowders (Fig. 2). For all-atom PEGs, we used 28-mer PEG polymers in five starting conformations sampled from MD simulations of PEG molecules in explicit solvent (26). All systems were solvated using the TIP3P water model, and ions were added using MMTSB (27). Explicit water molecules were placed with at least 9 Å margin from the protein atoms. Random water molecules were substituted with Na^+ and Cl^- ions according to an ionic strength of ~20 mM (9). Two additional Cl^- ions were added to the NS3/4A systems for charge neutrality. NS3/4A in explicit water and ions consisted of ~129,000 atoms in a box volume of 110 $Å^3$.

To generate the crowded systems, 130 single-atom crowders were placed around NS3/4A in random positions, resulting in three sets of crowder locations. Each set of one-sphere crowders was then substituted with either CG crowders or all-atom PEGs (each time randomly selecting one of five all-atom PEG conformations). The crowders were added to the NS3/4A starting structure. This resulted in crowder volume fractions of 10–20% depending on the system. Simulated systems consisted of ~250,000 atoms with all-atom PEGs and ~121,000 atoms with CG crowders. The systems containing all-atom PEGs were energy minimized in vacuum before adding water molecules to eliminate any clashes from placing PEGs around NS3/4A. The peptide was simulated either in explicit solvent (~21,000 atoms) or in explicit solvent in the presence of 16 CG crowders added at random locations (~26,000 atoms). Other simulation conditions were set as for NS3/4A.

Crowder models

MD simulations were performed for two crowder models as shown in Fig. 2. The PEG 28-mers in all-atom representation reflect the conditions used in experiments of NS3/4A activity upon crowding (9) (Fig. 2 *A*). Starting conformations were taken from the MD simulations of Lee et al. (26). The CHARMM36 CGenFF force field parameters were combined with modified torsion angles (26). Because PEGs are hydrophilic, favorable interactions with polar groups on the surface of NS3/4A are possible. The second type of crowder is a CG model (Fig. 2 *B*) that emphasizes the volume-exclusion effect while minimizing favorable interactions with the protein surface.

When designing the CG crowder model, a simple idea is to use one-atom spheres with a radius according to crowder size. However, it is not computationally efficient to surround large CG crowders with atomistic water molecules because a large cutoff distance for nonbonded interactions is necessary to cover the distance between two centers of large interacting spheres. Therefore, an alternative bead-shell model was used. Bead-shell crowder models appeared in 2003 in one of the first simulations of crowding that investigated the escape of a CG protein from GroEL using Brownian dynamics simulations with implicit water (28). The crowders represented Ficoll and interacted via the repulsive part of the Lennard-Jones (LJ) potential and charges placed on the surface atoms. A similar bead-shell crowder model was also used in 2012, in the simulations of folding of a short peptide in explicit TIP4P water (29).

Our bead-shell model used here consists of 42 carbon-sized pseudoatoms distributed almost evenly on the surface of a sphere. The additional large pseudoatom in the center of a crowder stabilizes the spherical structure (Fig. 2 *B*) and prevents collapse due to van der Waals interactions between surface atoms. The mass of the pseudoatoms was assigned so that the total CG crowder mass is 1296 Da, equal to the mass of a 28-mer PEG. The mass of each surface atom was set to 25 Da and of the central atom to 246 Da. The masses were assigned to reflect the size distribution of the particles (see Supporting materials and methods, Section S1 for the parameter file). Heavier central atoms also result in reduced fluctuations of the crowder shape. The radius of our CG crowders corresponds to the average hydrodynamic radius of PEG, which is 7.7 Å (26).

Although interactions between the individual CG crowders were set as purely repulsive, the crowder-protease interactions follow an LJ potential with repulsive and attractive parts. The parameters of the surface pseudoatoms were set equal to those of PEG carbons (Supporting materials and methods, Section S1). However, the CG crowder pseudoatoms are not connected by bonds. The NAMD (30) bond exclusion function requires that all the excluded atoms be located within neighboring patches. This is why the bonds in CG models cannot be much longer than bonds in proteins. Three

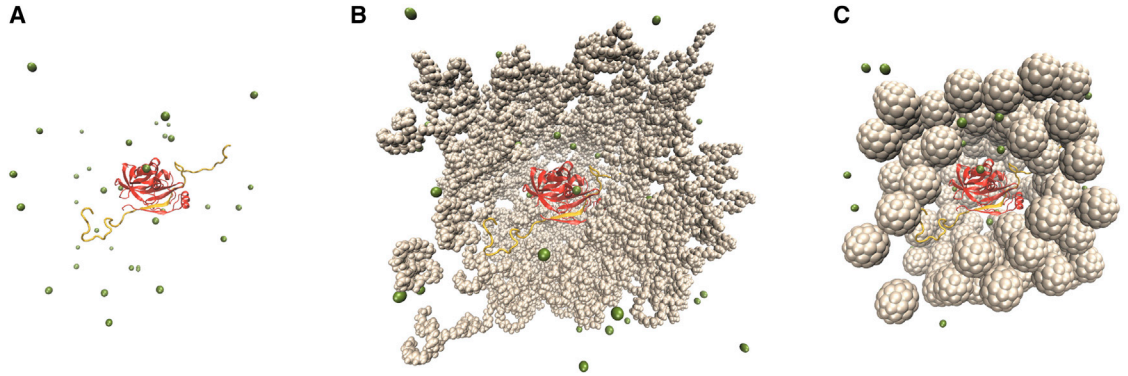

FIGURE 3 Simulated systems including NS3/4A. (*A*) NS3/4A surrounded by ions. (*B*) NS3/4A surrounded by all-atom 28-ethylene glycol molecules and ions. (*C*) NS3/4A surrounded by CG crowders and ions. For clarity, the water molecules are not shown, but they were included in the simulations. NS3 is shown in red, NS4A in orange, ions in green, and crowders in gray. To see this figure in color, go online.

approaches to pseudobond representation were tested: NBTables, extra bonds, and substitutions of bonds with a strong LJ potential. The third approach proved to be most practical and was implemented in our model.

MD simulations

All starting systems containing the protease or peptide mimicking the N-terminal segment of the cofactor were energy minimized over 3000 steps via steepest descent. Next, water molecules and ions were thermalized by gradually increasing the temperature from 10 to 310 K, running 25 ps of simulation at each temperature with harmonic restraints of 10 kcal/mol · Å^2 imposed on solute atoms. During subsequent equilibration, the positional restraints on the solute atoms were gradually weakened in six stages (of 25 ps each) with force constants k set to 10, 5, 2, 1, 0.1, and 0 kcal/mol · Å^2. Both heating and equilibration were carried out in the NVT ensemble with an integration time step of 1 fs. During an additional equilibration step over 25 ps, the ensemble was switched to NPT, and the time step was increased to 2 fs. For the protein in explicit water and with all-atom or CG crowders, five 500 ns production simulations were performed that differed in the starting velocities or crowder initial positions. For the peptide starting from helical or extended forms and with or without CG crowders, three sets of 1000 ns production simulations were carried out. The production simulations were performed in the NPT ensemble with NAMD 2.11 (30) or openMM 7.4 (31) on GPUs. Temperature was controlled by a Langevin thermostat, and a pressure of 1 atm was maintained using a Langevin piston (32). Electrostatic interactions were calculated via particle mesh Ewald summation (33) with a 12 Å direct-space cutoff. In the simulations with the CG crowders, the "pairlistdist" parameter that specifies the maximal distance for constructing the nonbonded interaction pair list was increased to 17 Å. This prevented the overlap of CG crowders. All bonds with hydrogen atoms were constrained with the SHAKE algorithm (34) to allow a 2 fs time step. The simulated NS3/4A systems are shown in Fig. 3. The dynamics from representative parts of the trajectories is illustrated in Video S1 (all-atom PEGs) and Video S2 (CG crowders). Basic trajectory analysis such as the calculation of root mean-square deviations (RMSDs), root mean-square fluctuations (RMSFs), radii of gyration (Rg), and secondary structure analysis was carried out using VMD (35). RMSD and RMSF were calculated for Cα atoms with respect to the minimized starting and average structures, respectively. All errors shown are the standard errors of the mean (SEM). Mean helicity in the NS4A N-terminus was estimated using VMD based on the number of frames in which the NS4A N-tail adopted an α- or 3_{10}-helix (normalized with respect to the total number of frames) according to STRIDE (36). In this analysis, only the last 250 ns of the production trajectories were used to allow sufficient time for helix formation. p-values were estimated based on a two-sample t-test to establish significance when comparing between water and crowded environments.

Force field parameters

The CHARMM36m force field (37) was applied because it is suitable for both folded and disordered protein elements, such as the unstructured NS4A tails. Because we observed PEG aggregation in initial simulations (Fig. S2), inconsistent with the known high solubility of this polymer (38), we scaled the ϵ parameter of the LJ potential for interactions between the water and other molecules by a factor of 1.09 (39), thereby increasing the hydrophobicity of the solutes. Such a modification was previously shown to restore realistic diffusion properties of overly aggregating peptides (39–41); this also proved successful here in preventing PEG aggregation and restored the expected high PEG solubility (Fig. S3). Scaled water interactions were applied in all MD simulations described here. In the simulations without crowding, the force field modifications increased the occurrence of conformations with larger Rg and also affected the stability of the NS4A helix that formed at the N-terminus (Figs. S4 and S5).

Diffusion coefficients

Translational diffusion was calculated based on the mean-square displacements (MSD) of the centers of mass of NS3 and crowders.

$$MSD(\tau) = \langle \left(\vec{r}(t+\tau) - \vec{r}(t) \right)^2 \rangle, \tag{1}$$

where r is the position of the molecule in time t and τ are the lag times between the positions. First, diffusion coefficients D_0 were calculated from the slopes of a linear fit to $MSD(\tau)$ according to the Einstein relation

$$D_0 = \frac{MSD(\tau)}{6\tau}. \tag{2}$$

Second, D_0 was corrected for the periodic boundary condition (PBC) artifacts (42) by adding the $D_{t,PBC}$ correction term calculated according to

$$D_{t,PBC} = \frac{Tk_B}{6L\pi\eta}\left(\zeta - \frac{4\pi R_h^2}{3L^2}\right) \tag{3}$$

and

$$\eta = \eta_w(1 + 2.5\phi), \tag{4}$$

where $\zeta = 2.837$, k_B is the Boltzmann constant, T is the temperature equal to 310 K, L is the length of the simulation box, η is the shear viscosity of the solvent, and R_h is the hydrodynamic radius of a molecule calculated for

NS3/4A with HYDROPRO (43) ($R_{NS3/4A} = 29$ Å), and the average radius of a PEG molecule R_{PEG} is equal to 7.7 Å (26). The shear viscosity of the solvent in crowded systems was calculated based on pure water viscosity, η_W, and the volume fraction of PEG crowders, ϕ.

Third, to account for reduced viscosity with the TIP3P water model used here, the PBC-corrected diffusion coefficients $D_{t,PBC}$ were further scaled with the factor of 3.08/8.9, the ratio between the shear viscosity of the TIP3P water model 0.308 cP relative to the experimental value of 0.89 cP for the viscosity of bulk water. Thus, the final double-corrected translational diffusion coefficients, D_t, are calculated as

$$D_t = (D_0 + D_{t,PBC}) \times \frac{3.08}{8.9}. \tag{5}$$

Rotational diffusion coefficients for NS3 were calculated based on rotational correlation functions (44) using the MMTSB toolset (27). A trajectory with random vectors was generated and merged with the trajectory of the centered NS3 structure. By fitting NS3 to the reference starting conformation, the vectors were rotated along with the protease, and the average correlation function was calculated for the vectors. Correlation times τ_r were generated by fitting the correlation function to a single exponential function $f = exp\left(\frac{-x}{\tau_r}\right)$. Rotational diffusion coefficients D_r are related to τ_r by $D_r = \frac{1}{6\tau_r}$. The correction related to the altered shear viscosity of the TIP3P model was also applied to D_r (i.e., D_r was scaled by 3.08/8.9). A PBC correction was not applied to D_r because it is negligible (45).

(De)coupling of the translational and rotational diffusion was analyzed based on the comparison with the hard sphere (HS) model (46). The diffusion coefficients in the HS model were calculated based on effective HS volume fractions ϕ_{HS} (47,48) as follows:

$$\frac{D^L(\phi_{HS})}{D_0^L} \cong \frac{(1-\phi_{HS})^3}{1 + (3/2)\phi_{HS} + 2\phi_{HS}^2 + 3\phi_{HS}^3} \tag{6}$$

and

$$\frac{\tau_r(\phi_{HS})}{\tau_{r,0}} \cong \left[1 - 0.631\phi_{HS} - 0.762\phi_{HS}^2\right]^{-1}, \tag{7}$$

where D_0^L and $\tau_{r,0}$ are the translational diffusion coefficients and rotational correlation times derived from the MD analysis of the protease in water and $D^L(\phi_{HS})$ and $\tau_r(\phi_{HS})$ are their theoretical values calculated for the protease surrounded by ideal hard spheres. The ϕ_{HS} fractions are equal to $\phi_{HS} = \phi \times k$, where ϕ is the volume fraction of crowders calculated from the trajectories and k is a scaling parameter set to 1 to obtain ideal HS results.

Protease and crowder contacts

Conditional radial distribution functions (RDFs) describing the distribution of PEG molecules around NS3/4A with respect to the protease surface were obtained with a custom program that calculates the number of crowder atoms of a specified type found within the available volume at a given distance from the closest heavy atom of the protease.

The conformations of NS4A with respect to NS3 were characterized with a measure called the wrapping coefficient, which distinguishes whether the unstructured tails are wrapped around NS3 or maximally extended. The wrapping coefficient W is defined as

$$W = \frac{\left(\sum_{i=1}^{N} x_i\right) - s_{min}}{s_{max} - s_{min}}, \tag{8}$$

where x_i is the distance between the Cα atom of the i-th residue of the N- or C-terminal tail of NS4A (for N residues: 1–22 and 33–54, respectively) and a fixed atom in the center of mass of NS3 (i.e., the Cα atom of GLY141). s_{max} and s_{min} are the minimal and maximal distance sums for each tail in all production simulations. W is constructed so that $W = 0$ represents the conformation with the tail closely wrapped around the protease and $W = 1$ the conformation with the tail maximally extended.

The timescales of forming the protease-crowder and crowder-crowder contacts were calculated via correlation analysis and based on the contact function $P(\Delta t)$ that describes whether a contact present at time t_0 is still present at time $t_0 + \Delta t$ (39,49):

$$P(\Delta t) = \frac{1}{N-k}\frac{1}{N_p}\sum_{j=1}^{N-k}\sum_{i=1}^{N_p}\delta_i(t_j)\delta_i(t_j + \Delta t), \tag{9}$$

where N is the number of trajectory frames, Δt is the k-th time interval (Δt = k × 0.5 ns, k = 1000), Np is the number of molecule pairs, and the function $\delta_i(t)$ takes a value of 1 when a molecule pair i is in contact at time t and 0 when the distance between the molecules is longer than the contact cutoff of 5 Å. A double exponential function (Eq. 10) was fitted to the correlation function to obtain correlation times of contacts on shorter (τ_c^s) and longer (τ_c^l) timescales, with a corresponding weight S_c:

$$f(\Delta t) = S_c \times exp\left(\frac{-\Delta t}{\tau_c^s}\right) + (1 - S_c) \times exp\left(\frac{-\Delta t}{\tau_c^l}\right). \tag{10}$$

CD spectroscopy

The high-performance liquid chromatography-grade peptide with the sequence of KKGG STWVLVGGVLAALAAYCLTTGS GGKK (N → C), mimicking the N-terminal tail of NS4A, was purchased from Lipopharm.pl (Gdańsk, Poland). The flanking KKGG were added as solubility tags. PEG 600 and PEG 2000 were purchased from Alfa Aesar (Haverhill, MA), and Ficoll 400 from Sigma Aldrich (St. Louis, MO). CD spectra were recorded in water, in 10 mM phosphate buffer (pH 7.0), and in the presence of PEG 600, PEG 2000, or Ficoll 400 suspended in the phosphate buffer. In all CD experiments, the peptide concentration was 50 μM. The concentration of PEG crowders was 50 mg/mL and of Ficoll was 25 mg/mL because of problems with dissolving the peptide in Ficoll crowders. The CD spectra were collected using the Biokine MOS-450/AF-CD spectrometer with the Xe lamp. The acquisition time was 2 s with a resolution of 1 nm. Measurements were performed using a 0.1 cm cell, in the wavelength range 190–260 nm and at room temperature, with the high-tension values below 600 V. The presented CD spectra are the averages of three scans. Each biological experiment was conducted twice. The Savitzky-Golay (50) method was used to smooth the graphs.

RESULTS AND DISCUSSION

Crowder interactions with the protein

PEG-protein contacts and hydrogen bond frequencies (9) show a variety of interaction types, ranging from hydrophobic contacts to electrostatic interactions with polar amino acids. At times, transient hydrogen bonds formed between the oxygen atoms of the PEG polymer chain (acting as hydrogen acceptors) and protein side chains (Fig. 4 *A*) or protein backbone atoms (Fig. 4 *B*) (acting as hydrogen donors).

The distribution of crowder molecules around NS3 (Fig. 4 *C*) features a sharp peak at ~4.5 Å in the PEG crowder RDF, indicating a characteristic distance preferred by PEG

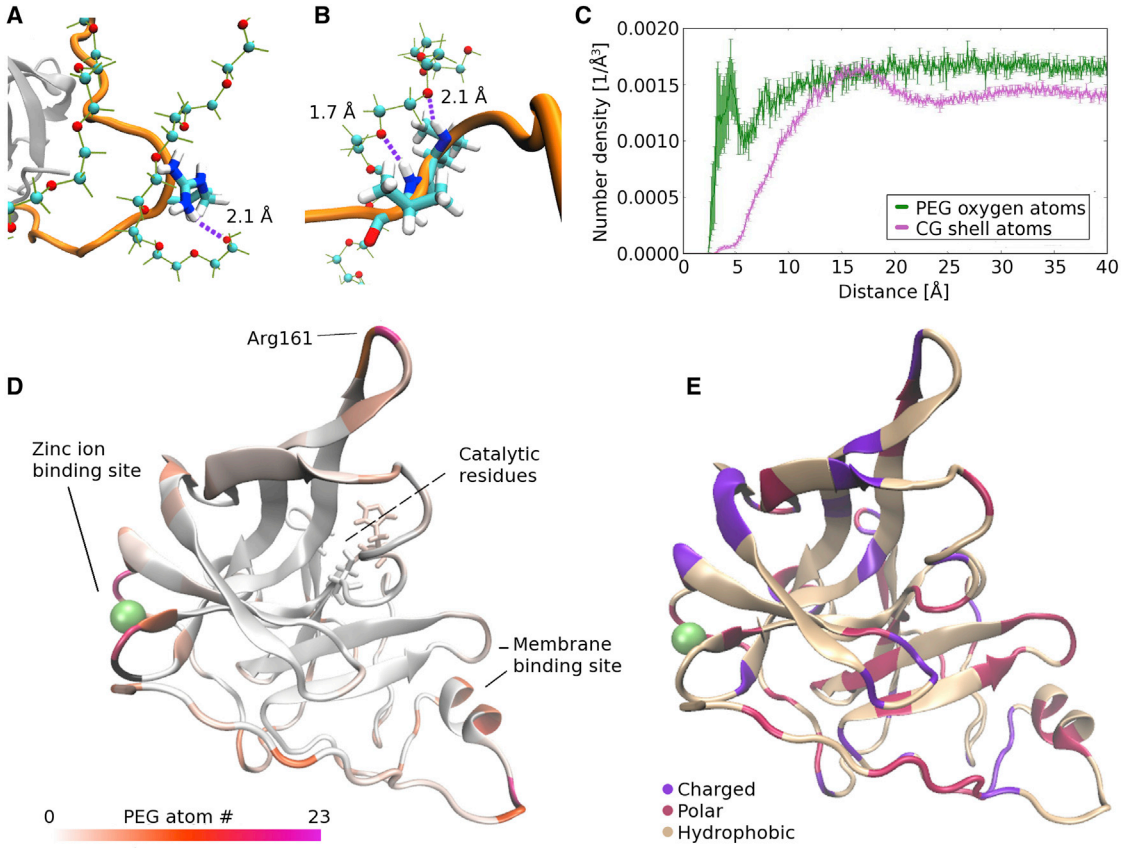

FIGURE 4 Crowder interactions with NS3. (*A*) Hydrogen bonding (*violet dashed lines* with hydrogen-acceptor distances) formed between the PEG oxygen and NS3 Arg amine. (*B*) Hydrogen bonds between PEG oxygens and NS3 peptide bond nitrogens. (*C*) RDF of the PEG oxygens and surface pseudoatoms of the CG crowders around NS3, averaged over five trajectories with mean ± SEM. RDF was normalized with respect to the volume fraction of the crowders and number of atoms per crowder (30 PEG oxygen atoms and 42 CG surface pseudoatoms). (*D*) NS3 colored according to the average number of PEG atoms found within 5 Å from a given residue (averages based on 100 snapshots taken at 5 ns intervals from a single 500 ns trajectory of NS3/4A with PEG crowders). (*E*) NS3 colored by amino acid type. To see this figure in color, go online.

oxygens around the protein. The location of the peak and the preceding slope suggest that the closest PEG-protein interactions involve hydrogen bonds.

Moreover, PEGs are not distributed evenly around the protease. NS3 colored according to the number of PEG atoms near the protein as shown in Fig. 4 *D* indicates that PEG interactions are reduced for the cavity-like parts of the NS3 surface. One of those cavity regions that is less populated with PEGs is the neighborhood of the NS3 active site. Crowders are distanced from the catalytic triad by over 7 Å, thereby leaving a PEG-free buffer zone large enough to fit an interacting peptide substrate (9). The most PEG-crowded regions near the protease surface correspond to the most solvent-exposed parts of the structure such as the zinc binding site rich in polar residues, the hydrophobic residues located in the short helix participating in membrane binding, and the vicinity of Arg161 in the β-sheet turn (Fig. 4, *D and E*). Although these regions are solvent accessible, no correlation was found between the amino acid type and the number of neighboring PEGs (Fig. 4, *D and E*). Given the complex spatial arrangement around the protease, PEGs at least partially resemble protein-like molecules with weak attractive interactions rather than inert crowders. This is consistent with similar conclusions from previous research (8).

The CG crowders are designed to mimic the volume-exclusion effect and lack the charge-charge interactions of the protein and PEG atoms, but they retain generic attractive interactions because of the van der Waals part of the LJ parameters of PEG carbon atoms used in the CG crowders. However, specific hydrogen bonds are not formed between the CG crowders and protein surface, so the CG crowders and protease interact less. This is reflected by the RDF showing a wide and flat peak at a distance of ∼17 Å (Fig. 4 *C*). Thus, the CG crowders mostly model inert crowders that restrict accessible volume.

Crowding reduces diffusion of the protease and crowders

Translational diffusion coefficients D_t and rotational correlation times τ_r for NS3 in various environments are given in Table 1. Both translation and rotational diffusion is

TABLE 1 Translational diffusion coefficients and rotational correlation times for NS3/4A in noncrowded and crowded environments

Environment	D_t (Å^2/ns)	τ_r (ns)
No crowders	6.98 ± 0.04	45.1 ± 2.5
PEG crowders	4.66 ± 0.01	76.7 ± 7.5
CG crowders	4.85 ± 0.05	63.8 ± 2.3
HS model	4.61	52.3

Translational diffusion coefficients, D_t; rotational correlation times, τ_r; mean ± SEM averaged over five production trajectories. HS values are $D^L(\phi_{HS})$ and $\tau_r(\phi_{HS})$ according to Eqs. 6 and 7 (51).

TABLE 2 Correlation times of protease-crowder and crowder-crowder contacts on two timescales, shorter τ_c^s and longer τ_c^l

Contact type	τ_c^s	τ_c^l	S_c
NS3-PEG	1.20 ± 0.26	29.78 ± 7.64	0.79
NS3-CG	0.43 ± 0.02	21.40 ± 0.41	0.93
PEG-PEG	0.45 ± 0.01	10.99 ± 0.46	0.74
CG-CG	0.03 ± 0.01	3.88 ± 0.04	0.99

Timescales based on fitting Eq. 10. Mean values ± SEM averaged over production trajectories. The weights S_c show that dominant contributions are from the shorter contact times.

reduced upon crowding. Translation is retarded similarly in the presence of CG and PEG crowders, by ∼40%, and similar to what is expected from an HS model (47,48,51). Rotational correlation times τ_r are increased by 70% with all-atom PEG crowders but less (40%) with CG crowders; both are significantly more than the HS prediction of a small increase by 15%. An increased retardation of rotational diffusion over the HS prediction indicates the presence of protein-crowder interactions and/or nonspherical solute shapes (51–53). The diffusion analysis was carried out for NS3, but the presence of the NS4A ligand adds deviations from a spherical shape because of at least partially extended N- and C-termini (see below). On the other hand, significant protein-crowder interactions are present with the all-atom PEG model as described above, based on the RDF analysis (Fig. 4) and previous work (9). Moreover, protein-crowder contacts persist longer with all-atom PEG crowders than with the CG crowders (see Table 2). This suggests that rotational diffusion is retarded more with all-atom PEGs versus CG crowders because of frequent transient clusters that persist long enough to affect rotational diffusion, similar to what has been observed with protein crowders (39).

The D_t-values calculated for the crowder molecules indicate that CG particles diffuse faster than all-atom PEGs, with $D_{t,CG} = 11.17 \pm 0.15$ and $D_{t,PEG} = 8.74 \pm 0.06$ Å^2/ns (Table S1). These results are again consistent with the atomistic PEGs forming interactions with the protease but also among themselves (Table 2). On the other hand, CG crowders show limited contacts with the protease and do not interact with each other, allowing faster diffusion.

In summary, PEG molecules transiently form clusters with the protease and with each other, whereas the CG crowders largely move independently, as they interact less with the protein and avoid each other.

NS3 remains stable, but crowding modulates NS4A flexibility

The radius of gyration, RMSD, and RMSF of NS3 vary only a little within the statistical uncertainties with and without crowders, with average RMSF values for NS3 below 1 Å (Table S2). Even though NS3 remains stable, its residue-based RMSF is redistributed by crowding (Fig. S6). The differences in NS3 flexibility occur mostly in loop regions and are consistently observed with both CG and all-atom PEG crowders (Fig. S6). The findings suggest a more complex response of the conformational dynamics of a globular protein subjected to crowders than what may be expected from simple volume-exclusion arguments, which would predict overall more compact and hence less-fluctuating structures.

NS4A is overall more dynamic compared to NS3. The central part of NS4A, bound to NS3, maintains a β-sheet (Fig. 5). However, regardless of the environment, the NS4A C-terminal tail relatively quickly wraps around the globular protease from the initial, almost fully extended conformations. The C-tail prefers conformations with a small wrapping coefficient, indicating that most amino acids are adherent to the NS3 surface (Fig. S7). Yet, the largely hydrophobic N-tail of the cofactor (which contains the proposed TM helix) adopts a broader range of conformations that depend on the type of crowders (Figs. 6 and S8). In the presence of CG crowders, the dominant conformation of the NS4A N-tail is a closely wrapped structure around NS3. The plots in Fig. 6 *A* show transitions between the expanded or wrapped states of the N-tail. Indeed, with CG crowders, once the N-terminal NS4A tail wraps around the protease, it stays wrapped until the end of the simulation. This result is in line with the theoretical predictions and earlier simulations of crowded systems (7,54,55), in which protein compaction is favored because of the excluded volume effect captured by the CG crowders.

In contrast, when surrounded by all-atom PEGs, the protein-crowder interactions allow many N-tail detachments, as in noncrowded environment (Figs. 6 and S8). This is confirmed by the average Rg of NS4A being larger in noncrowded and PEG environments (25.6 ± 1.2 and 25.7 ± 0.9 Å, respectively) than in CG crowders (22.4 ± 1.3 Å). In addition, the R_g distribution for the entire cofactor (Fig. S9) is broader for the noncrowded and PEG environments because of a large share of extended conformations for the N-terminus.

Crowding may stabilize a helical conformation in NS4A, priming it for membrane anchoring

The N-terminal tail of the cofactor mediates the membrane association of the NS3/4A complex by forming a TM α-

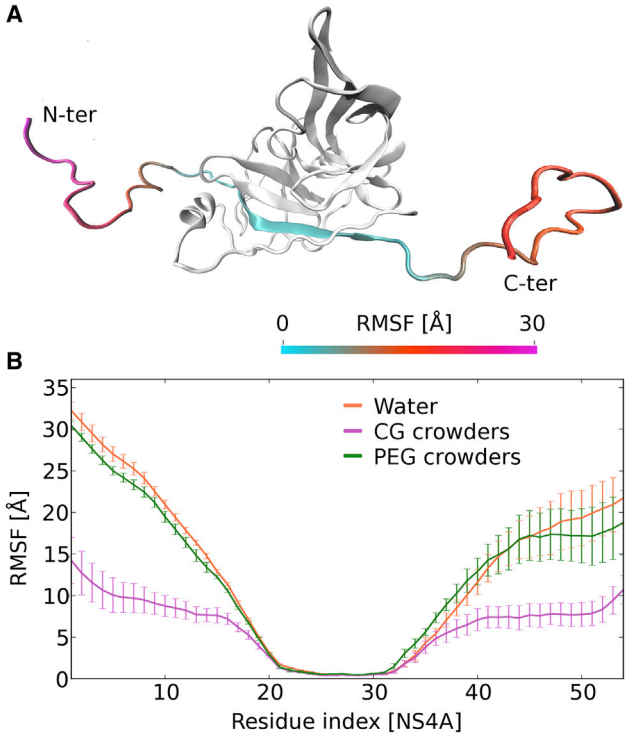

FIGURE 5 (*A*) The NS4A cofactor colored by the average RMSF values obtained from five simulations with all-atom PEG crowders, with NS3 shown in gray. (*B*) RMSF for NS4A in various environments (averages with mean ± SEM are over five simulations of each type). To see this figure in color, go online.

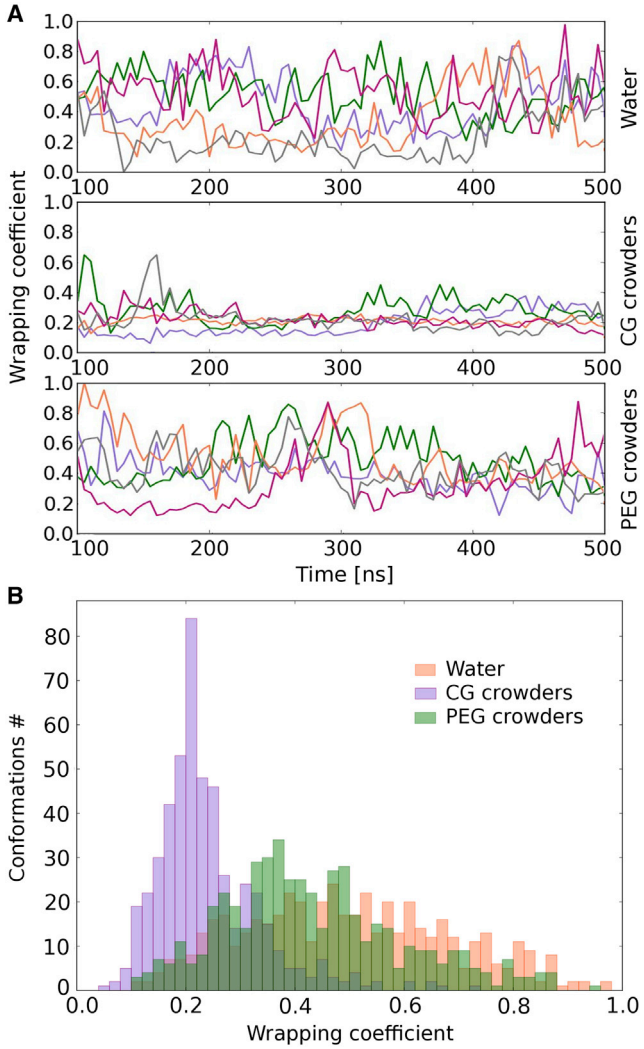

FIGURE 6 Wrapping coefficient of the N-terminal tail of NS4A shown as a function of the MD simulation time (*A*) and as the histogram of the number of conformations (*B*), with a bin size of W = 0.02) in the non-crowded and crowded environments. Low wrapping coefficient represents the conformation of the N-tail wrapped around NS3, and its values close to 1 represent an extended state. Colors in (*A*) correspond to five simulations of each type. To see this figure in color, go online.

helix. Circular dichroism and nuclear magnetic resonance experiments have confirmed a TM helix composed of up to 19 amino acids, in which residues Thr2, Trp3, Thr19, and Thr20 interact with the lipid headgroups at opposite sides of the membrane (19). The addition of a glycosylation acceptor site at the N-terminus of NS4A has led to experimental evidence that the helix traverses the ER membrane, with the N-terminus inside the ER lumen (19).

Although the NS4A N-tail remains largely unstructured in water, parts of it between residues 10 and 20 folded briefly into short helices (Fig. 7). Upon crowding, helical structures also formed in this region and were maintained for longer times (Fig. 7). More specifically, residues Ala12 to Tyr16 formed a particularly stable helix in one of each of the crowder simulations (Video S3). Based on statistical analysis, helix formation is more likely in the presence of the PEG crowders with moderate significance (p-value = 0.2) than with CG crowders (p-value = 0.35). Additional simulations of just the 22-residue N-terminal fragment of NS4A also show that helix formation is more likely in the presence of CG crowders (p = 0.2; Fig. S10), whereas an initially helical peptide is more stable in the crowded environment but starts to unfold in the noncrowded environment. Closer inspection of the all-atom PEG simulations did not indicate specific PEG-protein interactions that may correlate with helix formation. Moreover, because the helix also appears to be stabilized by CG crowders, it may be that the excluded volume effect exerted by the crowders is primarily responsible. However, the simulations are too short to establish unambiguously whether crowding shifts the equilibrium toward a helical structure in the N-terminus of NS4A or whether the crowders primarily provide kinetic stabilization of a helical structure.

The stabilization of a helical conformation in the N-tail of NS4A in various environments is consistent with the CD experiments of Brass et al. (19) and ours. The CD spectra of Brass et al. (19), recorded for residues 1–22 of the NS4A N-terminus in the presence of various micelles, show bands corresponding to an α-helix. In addition, the spectra are similar for both the negatively charged sodium

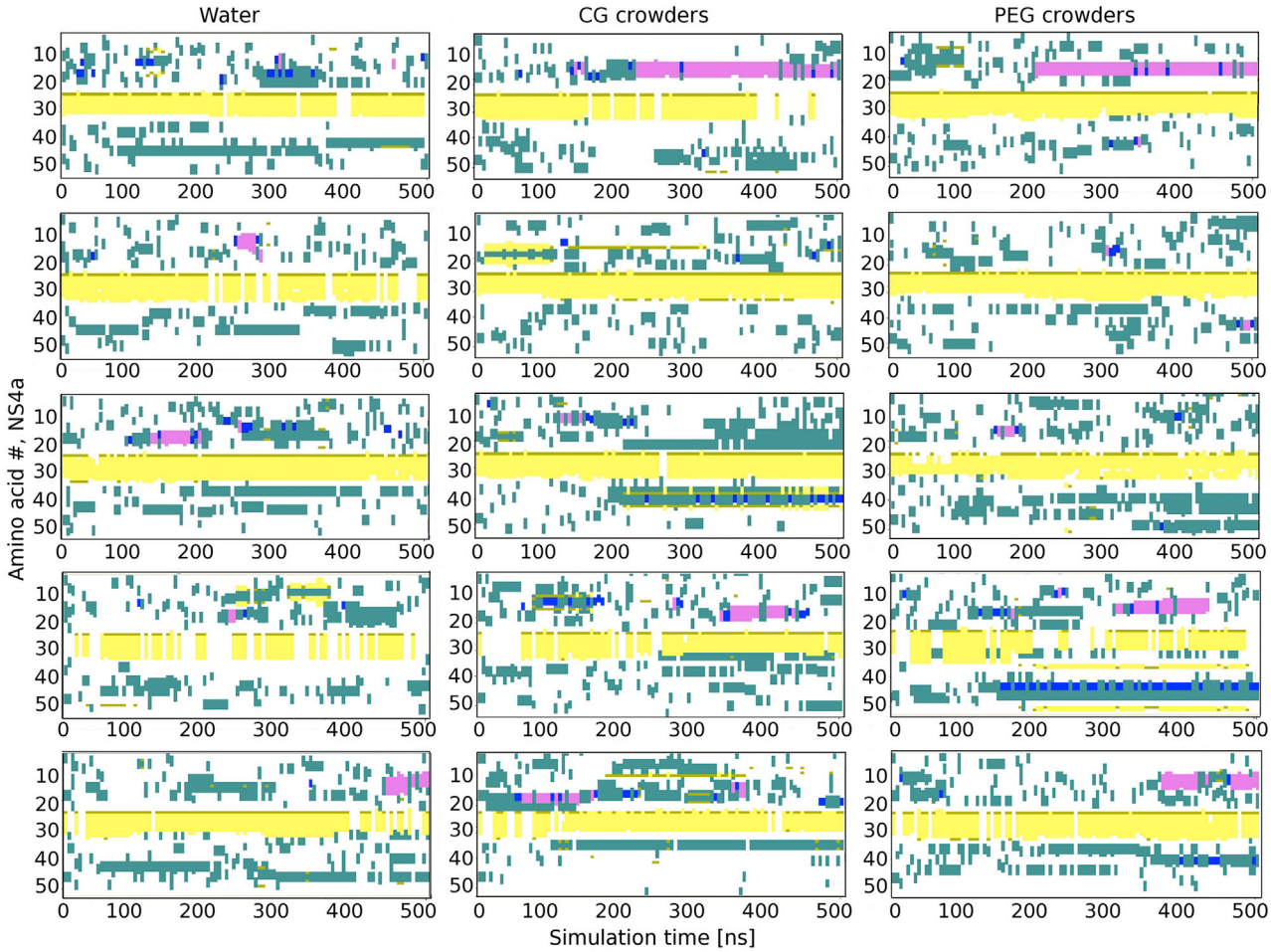

FIGURE 7 The secondary structures of NS4A formed in the simulations in water, with CG crowders, and with all-atom PEG crowders. Helical conformations are marked in pink or blue, β-strands in yellow, and turns in cyan. Each graph shows data from one MD trajectory. To see this figure in color, go online.

dodecyl sulfate (SDS) and neutral dodecylphosphocholine (DPC) micelles (19), suggesting that space restriction is a prevalent factor, rather than the electrostatic interaction between the peptide and micelle. Nevertheless, to test this hypothesis in the environment reflecting the simulated crowding agents, we performed CD experiments of the NS4A N-terminus in the presence of PEG and Ficoll crowders (Fig. 8). The CD spectra confirmed that both the interacting PEG and noninteracting CG crowders increase the helical content of the NS4A N-terminal peptide. Fig. 8 shows that in pure water, the peptide structure cannot be clearly identified (it is probably a mixture of various structures), but in the buffer, the CD spectrum intensity increases, and the α-helical spectral signatures start to appear (negative bands at 208 and 222 nm and a positive band at $\sim$192 nm). After incubation with crowders, the CD spectrum intensity increases even more, and the negative bands indicative of a helix become more evident. Whichever mechanism is at play, the main conclusion is that crowding appears to stabilize a helical conformation in the region of NS4A assumed to correspond to a TM helix when inserted into a membrane, thereby priming the NS4A N-terminus for membrane insertion to anchor the NS3/4A complex near the membrane.

Stable membrane binding of the NS3/4A complex is achieved by forming a three-point contact site involving the NS4A N-terminal TM helix and two elements of NS3: the 38–40 loop and the 12–23 helix (19) (Fig. 1). Based on partially folded NS4A structures extracted from the trajectories with all-atom and CG crowders, the helical fragment in NS4A forms in the proximity of the NS3 fragments that are expected to contact the membrane (Fig. 9). The spatial location of this helical fragment and consistent folding within the same range of highly conserved residues suggest that its formation in solution might play the role of a TM helix precursor. Crowding, moreover, as encountered in cells upon viral infections, seems to stabilize such a precursor.

According to Brass et al. (19), NS4A inserts into the membrane after insertion of the amphipathic 12–23 helix

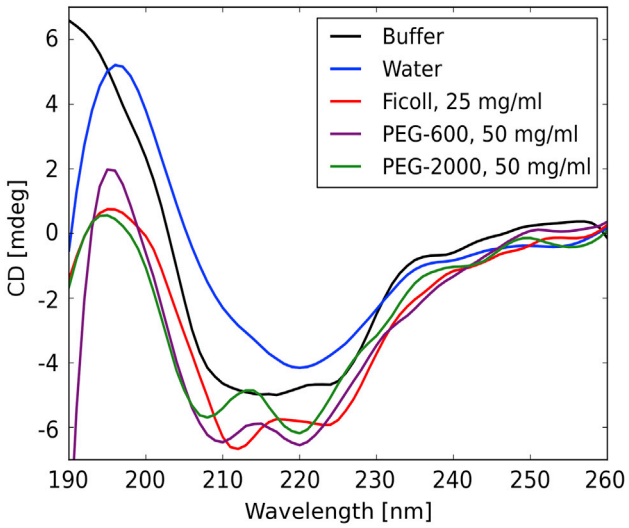

FIGURE 8 CD spectra of the N-terminal tail of NS4A in diluted (water and phosphate buffer) and crowded (with PEG and Ficoll) environments. To see this figure in color, go online.

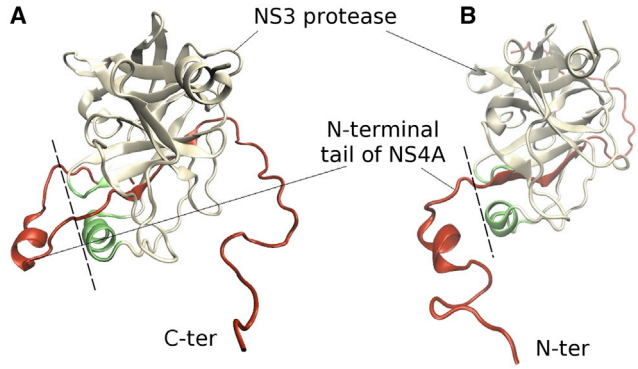

FIGURE 9 Helical fragment formed in the presence of CG (*A*) and all-atom PEG (*B*) crowders shown in representative trajectory conformations at $t = 290$ ns. Two NS3 membrane contact sites, in the 38–40 loop and the 12–23 helix of NS3, are shown in green. The dashed line schematically indicates the membrane position. To see this figure in color, go online.

of NS3 via an unusual mechanism of spontaneous insertion, with a possible role of highly conserved amino acids that are prevalent in the N-tail. Thus, the role of the NS4A TM helix precursor observed in our simulations, might be to facilitate the initial adsorption onto the membrane surface similar to a mechanism described for the adsorption of amphipathic helices. The sequence of the precursor helix, Ala-Leu-Ala-Ala-Tyr, suggests a membrane topology with a Tyr residue interacting with the lipid headgroups, in which the hydrophobic residues would be oriented toward the membrane core. The adsorption precursor could be followed by spontaneous helix formation on the membrane-water interface, similar to a mechanism described for polyleucine as simulated by Ulmschneider et al. (56). In that simulation, the unfolded peptide quickly adsorbed onto the membrane interface and subsequently folded spontaneously into a helix in the membrane.

In summary, the TM helix insertion mechanism proposed for the N-terminal tail of NS4A under crowded cellular conditions would consist of a crowding-induced initial folding of the helical precursor, adsorption onto the membrane surface assisted by NS3-membrane interactions, and finally spontaneous complete TM helix formation at the membrane interface and transition to a transmembrane conformation. Although a full analysis of the proposed mechanism is beyond the scope of this work, it could be examined via simulations in future studies to develop more specific hypotheses to be tested in an experiment assessing the effects of crowding on the NS3/4A activity.

CONCLUSIONS

The effects of crowding on biomolecular structure and dynamics are partially understood, but much less is known about how crowding in cellular environments may directly impact biological function. In this study, crowding effects on the conformational dynamics of the NS3/4A complex from HCV are described from MD simulations in water and in the presence of crowders. The crowders were modeled to represent PEG to allow comparisons with experiments. With an all-atom model of PEG, we found partially attractive interactions that are reminiscent of protein-protein interactions in crowded environments. Therefore, PEG may serve as a generic mimic of weakly interacting protein crowders in both simulations and experiment. The apparently protein-like behavior of PEG might also explain the results of our earlier experiments (9), in which we found that PEG and Ficoll affect the enzymatic activity of NS3/4A. According to those experiments, Ficoll, which is typically described as an ideal inert crowder because of the lack of interactions with proteins, enhanced the protease activity. In contrast, PEG considerably slowed down enzyme activity, an effect that may be expected because of PEG-protease interactions. Therefore, PEG might be a more realistic crowder of protein crowders in the cell than generally believed but easier to use experimentally than protein crowders, especially at higher concentrations.

We found that the globular NS3 protease is only weakly affected by the presence of crowders, mostly in the form of altered loop dynamics, whereas NS4A with flexible N- and C-terminal tails was more sensitive to the presence of the crowders. The most interesting observation was the finding that crowding appears to stabilize a short helical fragment in its N-terminal tail involving residues known to form a TM helix while positioning that helix next to membrane-interacting parts of NS3 as a likely precursor to TM helix insertion and subsequent anchoring of NS3/4A. This is likely important in priming NS3/4A for its function during viral replication. There is much left to be done via simulations and experiments to develop and test hypotheses for the specific mechanism of how NS3/4A adsorbs and anchors to membranes. This is a subject for future studies.

We used here two types of crowders to disentangle two main effects of crowding: nonspecific protein-crowder interactions and the excluded volume effect. Both were found to stabilize the helical fragment that folded in the N-terminal tail of NS4A, suggesting that the excluded volume effect is sufficient. Considering only the volume-exclusion effect via the CG crowders did, however, lead to more compact conformations, with the NS4A tails interacting more closely with NS3, whereas at least the N-terminal tail remained more flexible and able to detach in the presence of the all-atom PEG crowders. Such flexibility in the presence of crowders may be similar to what is observed in the presence of protein crowders in the cell and is likely needed for the NS4A N-terminus to insert into the membrane after the initial helix formation. As we found in CD experiments of the N-terminus of NS4A, both PEG and Ficoll crowders induce the formation of a helical structure.

The analysis presented here suggests that cellular crowding may act as an enhancer of biological function, in this case assisting with NS3/4A TM helix precursor formation and positioning near the membrane surface to facilitate membrane anchoring and ultimately facilitating viral replication. Such a role of crowding expands previous findings in which protein stability, dynamics, and enzyme rates were modulated by crowding and may be just the beginning of realizing an even broader role of crowding in supporting biological function in cellular environments.

SUPPORTING MATERIAL

Supporting material can be found online at https://doi.org/10.1016/j.bpj.2021.07.008.

AUTHOR CONTRIBUTIONS

N.O., M.F., and J.T. designed research. N.O. parameterized the CG crowder model. N.O. and M.F. performed simulations and analyzed data. N.O., M.F., and J.T. wrote the manuscript. J.T. supervised research and provided resources.

ACKNOWLEDGMENTS

N.O. and J.T. thank Dr. Monika Wojciechowska for helping with the CD experimental setup.

N.O. and J.T. thank support from the National Science Centre, Poland, UMO-2016/23/B/NZ1/03198. M.F. acknowledges support from the Polish National Agency for Academic Exchange (Ulam programme, PPN/ULM/2019/1/00060/DEC/1). Simulations were performed at the University of Warsaw: Centre of New Technologies and Interdisciplinary Centre for Mathematical and Computational Modelling (grants GB73-3 and GB77-7).

REFERENCES

1. Zhou, H. X., G. Rivas, and A. P. Minton. 2008. Macromolecular crowding and confinement: biochemical, biophysical, and potential physiological consequences. *Annu. Rev. Biophys.* 37:375–397.
2. Rivas, G., and A. P. Minton. 2016. Macromolecular crowding in vitro, in vivo, and in between. *Trends Biochem. Sci.* 41:970–981.
3. Latshaw, D. C., M. Cheon, and C. K. Hall. 2014. Effects of macromolecular crowding on amyloid beta (16-22) aggregation using coarse-grained simulations. *J. Phys. Chem. B.* 118:13513–13526.
4. Kim, Y. C., R. B. Best, and J. Mittal. 2010. Macromolecular crowding effects on protein-protein binding affinity and specificity. *J. Chem. Phys.* 133:205101.
5. Miller, C. M., Y. C. Kim, and J. Mittal. 2016. Protein composition determines the effect of crowding on the properties of disordered proteins. *Biophys. J.* 111:28–37.
6. Bille, A., K. S. Jensen, …, A. Irbäck. 2019. Stability and local unfolding of SOD1 in the presence of protein crowders. *J. Phys. Chem. B.* 123:1920–1930.
7. Harada, R., N. Tochio, …, M. Feig. 2013. Reduced native state stability in crowded cellular environment due to protein-protein interactions. *J. Am. Chem. Soc.* 135:3696–3701.
8. Nguemaha, V., S. Qin, and H.-X. Zhou. 2018. Atomistic modeling of intrinsically disordered proteins under polyethylene glycol crowding: quantitative comparison with experimental data and implication of protein-crowder attraction. *J. Phys. Chem. B.* 122:11262–11270.
9. Popielec, A., N. Ostrowska, …, J. Trylska. 2020. Crowded environment affects the activity and inhibition of the NS3/4A protease. *Biochimie.* 176:169–180.
10. Zhu, H., and J. M. Briggs. 2011. Mechanistic role of NS4A and substrate in the activation of HCV NS3 protease. *Proteins.* 79:2428–2443.
11. Geddawy, A., Y. F. Ibrahim, …, M. A. Ibrahim. 2017. Direct acting anti-hepatitis C virus drugs: clinical pharmacology and future direction. *J. Transl. Int. Med.* 5:8–17.
12. 2020. NS3/4A protease inhibitors. https://go.drugbank.com/categories/DBCAT002768.
13. El-Hage, N., and G. Luo. 2003. Replication of hepatitis C virus RNA occurs in a membrane-bound replication complex containing nonstructural viral proteins and RNA. *J. Gen. Virol.* 84:2761–2769.
14. Qin, S., and H. X. Zhou. 2013. Effects of macromolecular crowding on the conformational ensembles of disordered proteins. *J. Phys. Chem. Lett.* 4:3429–3434.
15. Banks, A., S. Qin, …, H. X. Zhou. 2018. Intrinsically disordered protein exhibits both compaction and expansion under macromolecular crowding. *Biophys. J.* 114:1067–1079.
16. Predeus, A. V., S. Gul, …, M. Feig. 2012. Conformational sampling of peptides in the presence of protein crowders from AA/CG-multiscale simulations. *J. Phys. Chem. B.* 116:8610–8620.
17. Bille, A., B. Linse, …, A. Irbäck. 2015. Equilibrium simulation of trp-cage in the presence of protein crowders. *J. Chem. Phys.* 143:175102.
18. Yan, Y., Y. Li, …, Z. Chen. 1998. Complex of NS3 protease and NS4A peptide of BK strain hepatitis C virus: a 2.2 A resolution structure in a hexagonal crystal form. *Protein Sci.* 7:837–847.
19. Brass, V., J. M. Berke, …, D. Moradpour. 2008. Structural determinants for membrane association and dynamic organization of the hepatitis C virus NS3-4A complex. *Proc. Natl. Acad. Sci. USA.* 105:14545–14550.
20. LaPlante, S. R., H. Nar, …, S. H. Kawai. 2014. Ligand bioactive conformation plays a critical role in the design of drugs that target the hepatitis C virus NS3 protease. *J. Med. Chem.* 57:1777–1789.
21. Abian, O., S. Vega, …, A. Velazquez-Campoy. 2010. Conformational stability of hepatitis C virus NS3 protease. *Biophys. J.* 99:3811–3820.
22. Pettersen, E. F., T. D. Goddard, …, T. E. Ferrin. 2004. UCSF Chimera–a visualization system for exploratory research and analysis. *J. Comput. Chem.* 25:1605–1612.
23. Berkholz, D. S., M. V. Shapovalov, …, P. A. Karplus. 2009. Conformation dependence of backbone geometry in proteins. *Structure.* 17:1316–1325.
24. Fiser, A., R. K. Do, and A. Sali. 2000. Modeling of loops in protein structures. *Protein Sci.* 9:1753–1773.

25. Shen, M. Y., and A. Sali. 2006. Statistical potential for assessment and prediction of protein structures. *Protein Sci.* 15:2507–2524.
26. Lee, H., R. M. Venable, …, R. W. Pastor. 2008. Molecular dynamics studies of polyethylene oxide and polyethylene glycol: hydrodynamic radius and shape anisotropy. *Biophys. J.* 95:1590–1599.
27. Feig, M., J. Karanicolas, and C. L. Brooks, III. 2004. MMTSB Tool Set: enhanced sampling and multiscale modeling methods for applications in structural biology. *J. Mol. Graph. Model.* 22:377–395.
28. Elcock, A. H. 2003. Atomic-level observation of macromolecular crowding effects: escape of a protein from the GroEL cage. *Proc. Natl. Acad. Sci. USA.* 100:2340–2344.
29. Kurniawan, N. A., S. Enemark, and R. Rajagopalan. 2012. Crowding alters the folding kinetics of a β-hairpin by modulating the stability of intermediates. *J. Am. Chem. Soc.* 134:10200–10208.
30. Phillips, J. C., R. Braun, …, K. Schulten. 2005. Scalable molecular dynamics with NAMD. *J. Comput. Chem.* 26:1781–1802.
31. Eastman, P., J. Swails, …, V. S. Pande. 2017. OpenMM 7: rapid development of high performance algorithms for molecular dynamics. *PLoS Comput. Biol.* 13:e1005659.
32. Feller, S., Y. Zhang, …, B. Brooks. 1995. Constant pressure molecular dynamics simulation: the Langevin piston method. *J. Chem. Phys.* 103:4613–4621.
33. Darden, T., D. York, and L. Pedersen. 1993. Particle mesh Ewald: an N log(N) method for Ewald sums in large systems. *J. Chem. Phys.* 98:10089–10092.
34. Ryckaert, J., G. Ciccotti, and H. Berendsen. 1977. Numerical integration of the cartesian equations of motion of a system with constraints: molecular dynamics of n-alkanes. *J. Comput. Phys.* 23:327–341.
35. Humphrey, W., A. Dalke, and K. Schulten. 1996. VMD: visual molecular dynamics. *J. Mol. Graph.* 14:33–38, 27–28..
36. Frishman, D., and P. Argos. 1995. Knowledge-based protein secondary structure assignment. *Proteins.* 23:566–579.
37. Huang, J., S. Rauscher, …, A. D. MacKerell, Jr. 2017. CHARMM36m: an improved force field for folded and intrinsically disordered proteins. *Nat. Methods.* 14:71–73.
38. Özdemir, C., and A. Güner. 2007. Solubility profiles of poly(ethylene glycol)/solvent systems, I: qualitative comparison of solubility parameter approaches. *Eur. Polym. J.* 43:3068–3093.
39. Nawrocki, G., P. H. Wang, …, M. Feig. 2017. Slow-down in diffusion in crowded protein solutions correlates with transient cluster formation. *J. Phys. Chem. B.* 121:11072–11084.
40. Petrov, D., and B. Zagrovic. 2014. Are current atomistic force fields accurate enough to study proteins in crowded environments? *PLoS Comput. Biol.* 10:e1003638.
41. Best, R. B., W. Zheng, and J. Mittal. 2014. Balanced protein-water interactions improve properties of disordered proteins and non-specific protein association. *J. Chem. Theory Comput.* 10:5113–5124.
42. Yeh, I., and G. Hummer. 2004. System-size dependence of diffusion coefficients and viscosities from molecular dynamics simulations with periodic boundary conditions. *J. Phys. Chem. B.* 108:15873–15879.
43. Ortega, A., D. Amorós, and J. García de la Torre. 2011. Prediction of hydrodynamic and other solution properties of rigid proteins from atomic- and residue-level models. *Biophys. J.* 101:892–898.
44. Wong, V., and D. A. Case. 2008. Evaluating rotational diffusion from protein MD simulations. *J. Phys. Chem. B.* 112:6013–6024.
45. Linke, M., J. Köfinger, and G. Hummer. 2018. Rotational diffusion depends on box size in molecular dynamics simulations. *J. Phys. Chem. Lett.* 9:2874–2878.
46. Minton, A. P. 1998. Molecular crowding: analysis of effects of high concentrations of inert cosolutes on biochemical equilibria and rates in terms of volume exclusion. *Methods Enzymol.* 295:127–149.
47. van Blaaderen, A., J. Peetermans, …, J. K. G. Dhont. 1992. Long-time self-diffusion of spherical colloidal particles measured with fluorescence recovery after photobleaching. *J. Chem. Phys.* 96:4591–4603.
48. Koenderink, G. H., H. Zhang, …, G. Nägele. 2003. On the validity of Stokes-Einstein-Debye relations for rotational diffusion in colloidal suspensions. *Faraday Discuss.* 123:335–354, discussion 401–421.
49. Brunne, R. M., E. Liepinsh, …, W. F. van Gunsteren. 1993. Hydration of proteins. A comparison of experimental residence times of water molecules solvating the bovine pancreatic trypsin inhibitor with theoretical model calculations. *J. Mol. Biol.* 231:1040–1048.
50. Savitzky, A., and M. J. E. Golay. 1964. Smoothing and differentiation of data by simplified least squares procedures. *Anal. Chem.* 36:1627–1639.
51. Roos, M., M. Ott, …, K. Saalwächter. 2016. Coupling and decoupling of rotational and translational diffusion of proteins under crowding conditions. *J. Am. Chem. Soc.* 138:10365–10372.
52. Mereghetti, P., and R. C. Wade. 2012. Atomic detail brownian dynamics simulations of concentrated protein solutions with a mean field treatment of hydrodynamic interactions. *J. Phys. Chem. B.* 116:8523–8533.
53. Roos, M., S. Link, …, K. Saalwächter. 2015. NMR-detected brownian dynamics of αB-crystallin over a wide range of concentrations. *Biophys. J.* 108:98–106.
54. Candotti, M., and M. Orozco. 2016. The differential response of proteins to macromolecular crowding. *PLoS Comput. Biol.* 12:e1005040.
55. Zegarra, F. C., D. Homouz, …, M. S. Cheung. 2019. Crowding-induced elongated conformation of urea-unfolded apoazurin: investigating the role of crowder shape in silico. *J. Phys. Chem. B.* 123:3607–3617.
56. Ulmschneider, M. B., J. P. Ulmschneider, …, S. H. White. 2016. Spontaneous transmembrane helix insertion thermodynamically mimics translocon-guided insertion. *J. Am. Chem. Soc.* 138:10365–10372.